# High-performance superconducting photon number resolving detectors with 86% system efficiency at telecom range.

**MARIA MOSHKOVA,[1,2,*] ALEXANDER DIVOCHIY,[2,] PAVEL MOROZOV,[2] YURY VAKHTOMIN, [2,3] ANDREY ANTIPOV,[2] PHILIPP ZOLOTOV, [1,2] VITALY SELEZNEV,[2,3] MARAT AHMETOV,[2] AND KONSTANTIN SMIRNOV[1,2,3]**

[1]*National Research University Higher School of Economics, Moscow, DC 101000, Russia*
[2]*LLC "Superconducting Nanotechnology" (SCONTEL), Moscow, DC 119021, Russia*
[3]*Moscow State Pedagogical University, DC 119991, Russia*

**moshkova@scontel.ru*

**Abstract:** The use of improved fabrication technology, highly disordered NbN thin films, and intertwined section topology makes possible to create high-performance photon-number-resolving superconducting single-photon detectors (PNR SSPDs) that are comparable to conventional single-element SSPDs at the telecom range. The developed four-section PNR SSPD has simultaneously an 86% ±3% system detection efficiency, 35 cps dark count rate, ~2 ns dead time, and maximum 90 ps jitter. An investigation of the PNR SSPD's detection efficiency for multi-photon events shows good uniformity across sections. As a result, such a PNR SSPD is a good candidate for retrieving the photon statistics for light sources and quantum key distribution (QKD) systems.



## 1. Introduction

Currently, single-photon detectors are used in a variety of applications. The majority of these applications require both the high efficiency of detection devices and their temporal characteristics. Considering these demands, superconducting single-photon detectors (SSPDs) [1] usually outperform other types of detectors significantly when considering four key characteristics - system detection efficiency (SDE), dark count rate, dead time, and jitter. Moreover, these key characteristics comprising SSPD leadership are supported by SSPDs' wide operation wavelength range. These detectors have opened fundamentally new application possibilities [2]. The rapid increase in the use of SSPDs led to significant progress in its fabrication technology and, as a result, to the development of single-element SSPDs with ultimate characteristics, such as SDEs, approaching 100% [2-5].

Further research has determined a need for SSPD improvements via the production of multi-element devices. Such a configuration can distinguish the number of photons contained in one short optical pulse of radiation. At this moment proposed two types of PNR detectors where sensitive area of detectors divided to *k* sections and in type 1 it connected in parallel [6,7] and in type 2 in series [8]. Undoubtedly, quantum cryptography is one of the most promising application areas for such photon-number-resolving (PNR) detectors. The investigation of PNR detectors' capabilities and prospects for quantum cryptography has continued throughout the whole history of their development [9,10]. It is obviously that PNR detectors provide several prospective improvements for QKD systems, that is: a) they may enhance the information-carrying capacities of quantum channels, b) they enhance the security of the secret key through the detection of pulse-splitting attacks in which an eavesdropper can change the photon statistics of the pulses. The application of PNR SSPDs [6] in QKD systems has also become the object of study for many scientific and research

groups, demonstrating PNR SSPDs' prospects in such systems convincingly. Thereby, high-SDE PNR detectors can modernize the field of quantum optics. Unfortunately, current PNR SSPD characteristics are far from their ultimate values. Since the first demonstration, the SDEs of such detectors have not changed significantly and reach approximately 1% [6,8]. However, application of PNR detectors with low detection efficiency is extremely unpractical because the probability of the simultaneous occurrence of several random independent events is equal to the product of the probabilities of these events, leading to a vanishing efficiency value for multi-photon, higher-order operations. Although there has been progress in the development of high-performance single-element detectors over the past few years [3-5], creating a PNR SSPD with high detection efficiency would have a much higher practical potential for both quantum cryptography and other applications. The present work is devoted to the development and investigation of superconducting PNR detectors with high SDEs.

## 2. PNR SSPD fabrication technology

The sensitive area of the PNR detector is a set of parallel, 100-nm-wide superconducting NbN strips. A planar resistor is connected in series to each strip to prevent the cascading switching of strips when a detecting event appears in one of them [11]. For our devices, four parallel strips were distributed evenly over an area of 15x15 $\mu m^2$ (Figure 1). Nonetheless, the fabrication technology of PNR detectors and their topology allow the number of sections to be increased.

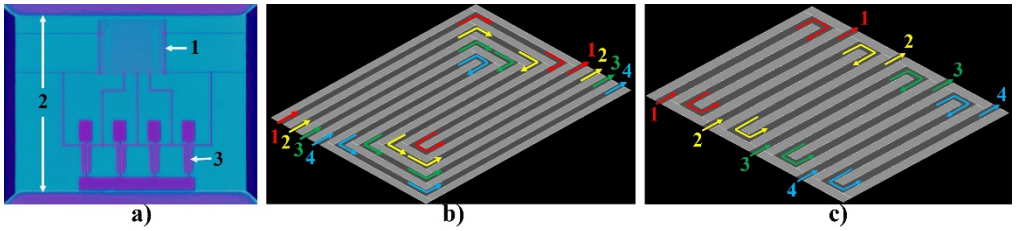


Fig. 1. a) PNR SSPD image obtained with optical microscope: 1 – sensitive area of PNR, 2 – contact pads, 3 – four planar resistors, light-blue area is the NbN film; b) schematic view of topology #1; c) schematic view of topology #2.

The thin NbN films for our devices were deposited over sapphire substrates with additional Au/$Si_3N_4$ optical cavity layers by reactive magnetron sputtering in an AJA International Orion series system [4]. The thickness of the films was around 6 nm, the surface resistance was in the range 600-700 Ohm/□, and the $T_C$ was 8-9 K. As was shown in [4] such parameters of NBN films correspond to high disordered films and allow to reach high quantum efficiency of the SSPD with saturated SDE($I_{bias}$) dependence. Parallel NbN strips were formed by e-beam lithography and subsequent plasma-chemical etching in a gas mixture of $SF_6$ and argon. Ti/Au resistors of ~150 Ohm each were fabricated using e-beam lithography followed by e-beam evaporation and the lift-off process. V-Cu contact pads were fabricated using photolithography followed by e-beam evaporation and the lift-off process. Photolithography and subsequent plasma-chemical etching were used in order to remove the superconducting film from undesired areas. The wafer was then cut into separate chips with a scriber.

Using the forementioned technology, we fabricated devices with the topologies that are shown schematically in Figure 1b (topology #1). We also compare our results with a previous study [12] which investigated the perfomance of detectors with a different topology - see Figure 1c (topology #2). The sensitive areas of each section in topology #2 are located in sequence one to another. All four sensitive areas of each section in topology #1 are distributed evenly over the 15x15 $\mu m^2$ area.

In order to reach a high SDE, we used an anti-reflection coating (ARC) technique, as described in our previous work [4]. Here, to obtain a high SDE for PNR detectors at the

telecom wavelength λ=1550 nm, we used the following layers: $Al_2O_3$ substrate 430μm /Au 80nm /$Si_3N_4$ 180nm /NbN 6nm /$Al_2O_3$ 230 nm /Si 105nm.

## 3. PNR SSPD operating principle

The equivalent circuit for a four-section PNR SSPD is presented in Figure 2a. Each separate section of the 4-PNR (four-section) detector is marked with a different color: $R_{hs}$ is the resistance of the NbN strip when a detecting event appears, $L_{kin}$ is the kinetic inductance of the NbN strip, $R_{is}$ is a planar Ti/Au resistor connected in series to each section to isolate adjacent sections, and K is a switch modeling the NbN strip state (the switch is closed in the superconducting state, while in the normal state, it is open). L and C indicate the inductance and capacitance of the bias-tee adapter, respectively. The superconductivity of the NbN strip that is biased with a current close to the critical value can be destroyed by the absorption of a single photon. The current flowing through this NbN strip starts redistributing between NbN sections connected in parallel and $R_{load}$. The additional resistance $R_{is}$ is connected to each section of the detector in order to minimize the bias current change in the superconducting sections and to avoid cascaded switching of all detector sections. However, sufficiently high resistance $R_{is}$ decreases the relaxation time of NbN strip between the normal and superconducting states (proportional to $L_k/(R_{is}+R_{load})$), which leads to an undesirable latching effect. We have adjusted the $R_{is}$ value to ~150 Ohm experimentally. The transition to the normal state of one NbN strip did not cause cascaded switching of other parallel sections, and, consequently, all sections of the detector were capable of simultaneous and independent detection of the absorbed photons at this resistance value.

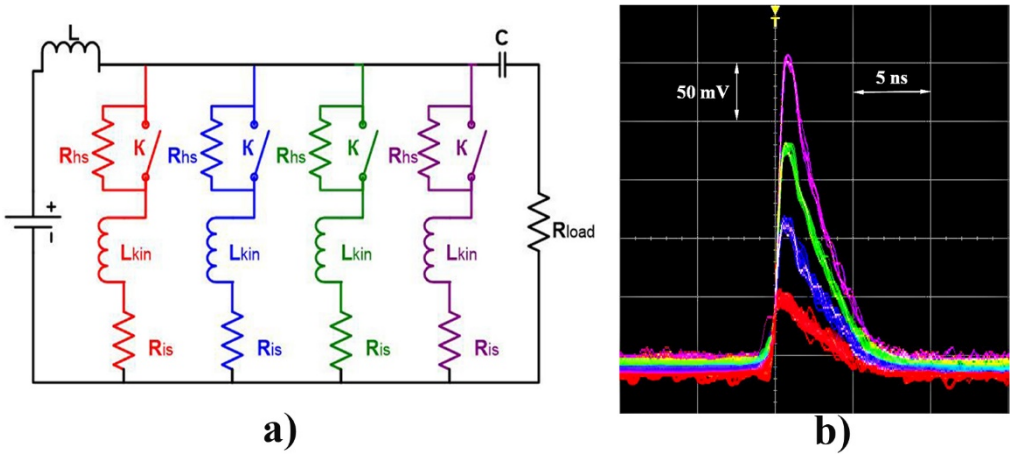


Fig. 2. a) Equivalent circuit of the 4-section PNR SSPD detector [Ref. 8, Fig.1b; Ref. 12, Fig.1], b) Oscilloscope traces of 4-PNR voltage pulse corresponds to different number of triggered sections colored separately.

The voltage appearing on the $R_{load}$ in this detector configuration is proportional to total current of the triggered NbN sections. In the case of similar values of current flow in each section, the amplitude of the output voltage pulse will be proportional to the number of photons recorded. The oscilloscope traces of the voltage pulse appearing in a different number of triggered sections of our 4-PNR SSPD is presented in Figure 2b.

## 4. Device characterization

### *4.1 Detection efficiency and dark count rate*

The manufactured 4-PNR SSPD was coupled with a standard telecom single-mode fiber SMF 28e and cooled in a closed-cycle refrigerator (Sumitomo RDK 101 D) with a minimum temperature of 2.3 K.

We measured the system detection efficiency of the 4-PNR SSPD in two ways - by using laser sources of continuous and pulsed radiation. We used the method and experimental setup described in detail in [4] for detection efficiency measurements using a continuous-wave (CW) source. It should be noted that established power of a CW laser of 0.128 pW at $\lambda$ = 1550 nm corresponds to $10^6$ photons per second. According to Poisson statistics, at such photon flux, the probability of more than one photon appearing in the time window of 2 ns (equivalent to the detector's dead time) is three orders lower than the probability of one photon event. This information allows us to neglect multiple photon detections. Therefore, this measurement via the CW source represent the average value of detection efficiency over all sections. The highest values of the system detection efficiency in a single-photon mode ($SDE_{1\_CW}$) we obtained was for sample #T1 (topology #1). The results are presented in Figure 3. The maximum $SDE_{1\_CW}$ was as high as 86±3% at bias currents of 27 μA, which corresponds to 35 cps of dark counts. Dependence of photon counts on pulse counter trigger level shown on fig.3b clearly demonstrate $10^{-3}$ probability of two-photon events for photon flux $10^6$ $s^{-1}$. Moreover, this results confirm that given 4-PNR SSPD have well enough isolation between section and thus free of cascade switching feature.

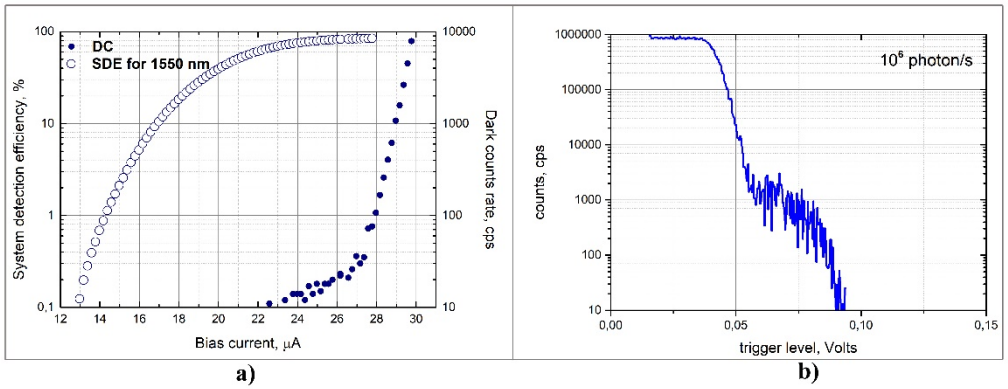


Fig. 3. a) Measured dependencies for SDE (CW laser) and Dark count rate vs. detector for the sample #T1, b) Measured dependence of photon counts vs. pulse counter trigger level for sample #T1 biased with 27 μA (~0.9•Ic).

The dependence of 4-PNR SSPD dark counts vs. the bias current is very typical for traditional single-element SSPD detectors [13], namely: a fast initial decay with decreasing bias current in region of 30 - 27 μA is due to the intrinsic dark counts of the detector and flattening at currents < 27 μA that is associated with detection of room-temperature background radiation passing through the fiber. The change point in the obtained dependence of dark counts for the detector #T1 (27 μA) corresponds to ~35 dark counts per second.

We have used a laser in the pulsed operation mode at $\lambda$ = 1550 nm and with repetition rate f = 10 MHz for measuring the efficiency of simultaneous detection of n-photons by a detector ($SDE_{n\_pulse}$). The photon number distribution in the laser pulse corresponds to Poisson statistics. We have measured the number of counts in a certain time (1s) depending on the trigger level of the pulse counter for two specific laser power values that correspond to the average number of photons in the pulse, $\mu$ = 0.1 and $\mu$ = 2. The dependences obtained for detector biased with 27 μA and for two values of $\mu$ shown on Fig. 4. These graphs have the expected stepwise appearance. At low triggering levels smaller than the amplitude of the detector pulse when one photon is detected, number of counted events corresponds to the sum of pulses with all amplitudes and include simultaneous triggering of one, two, three and four sections of the detector, i.e. $N_{exp}(1)+N_{exp}(2)+N_{exp}(3)+N_{exp}(4)$, where $N_{exp}(n)$ - the number of simultaneous triggering of *n* detector sections. At triggering levels higher than the amplitude of the detector pulse when one photon is detected, the counter begins to count $N_{exp}(2)+N_{exp}(3)+N_{exp}(4)$, which correspond to simultaneous triggering of two, three and four

sections of the detector and so forth. Thus, we can measure the number of counts which correspond to amplitudes higher than certain one, and can be written in the form of $M_{\exp}(n) = \sum_{i=n}^{k,k\geq n} N_{\exp}(i)$, where $k$ is the number of sections of the detector. Therefore, it is convenient to represent this dependence $M_{exp}(n)$ vs. the level of the voltage signal amplitude, i.e. in units of measurement corresponding to a single-photon operation of the detector (the upper axis in Figure 4). Since the detector has four independent sections, i.e. is capable of recording simultaneous absorption of up to four photons, these curves must have four distinct plateaus, as shown in Fig. 4b. Thus, for μ = 0.1, the probability of detecting 3 and 4 photons in the optical pulse is very small ($1.5 \times 10^{-4}$ and $1 \times 10^{-6}$), which makes it difficult to measure 3- and 4-photon processes because "steps" become blurred (Fig. 4a). When the average photon number in pulse increases to μ = 2, all 4 "steps" become easily distinguishable.

The theoretical expression of $N_{th}(n)$ may be calculated as:

$$N_{th}(n) = f \cdot \sum_{n\geq m} [p_0(\mu, m) \cdot P(m,n)] \quad (1)$$

where $p_0(\mu, m) = \frac{\mu^m \cdot e^{-\mu}}{m!}$ is the Poisson distribution, $f$ - is the repetition rate of the optical pulses, $P(m,n)$- is the probability of simultaneous triggering of $n$ detector sections when $m$ photon falls onto the detector, which may be defined as:

$$P(m,n) = \sum_{m_1,m_2,\ldots,m_k} \frac{m!}{(\prod_{i=1}^{k} m_i!) \cdot (m - \sum_{i=1}^{k} m_i)!} \cdot (\prod_{i=1}^{k} \eta^{m_i}) \cdot (1 - k \cdot \eta)^{m_{k+1}}, \quad (2)$$

Where $\eta$ - is the detection efficiency of each section, $m_i$ - is the number of photons absorbed by the $i$-th section. When summing in the formula (2), we choose $m_i$ in such a way that every $n$ sections absorb at least one photon and every $k$-$n$ sections absorb no photons. Paul et al. [14] gave the similar relation for detectors of unity efficiency. In our case we generalized relation for detectors with arbitrary detection efficiency.

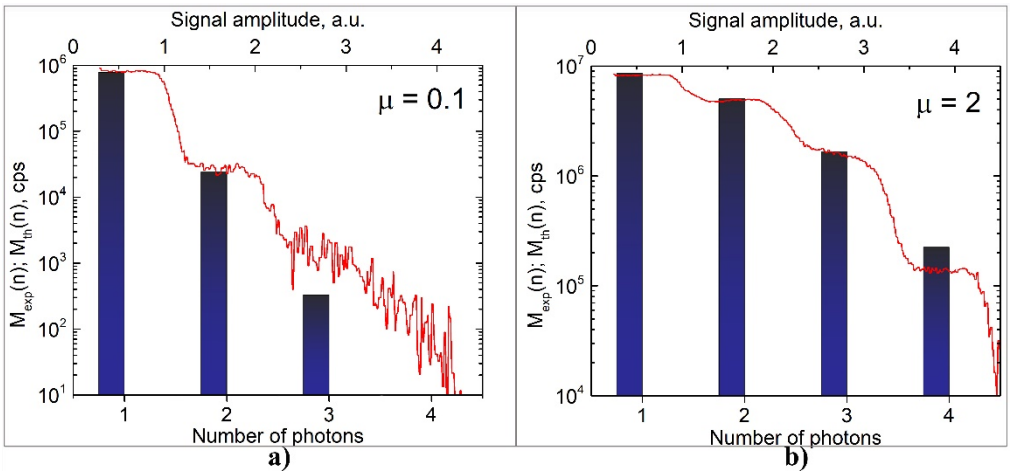


Fig. 4. Dependencies of 4-PNR SSPD detector counts on the amplitude of the output voltage pulse (trigger level) for sample #T1: $M_{exp}(n)$ (solid curve), $M_{th}(n)$(bars) for a) μ = 0.1 and b) μ= 2.

For detectors of unity efficiency ($k \cdot \eta = 1$) it is possible to calculate maximum values $N_{max}(n)$ of $N_{th}(n)$ from (1) and determine the detection efficiency as $SDE_{n\_pulse} = N_{exp}(n)/N_{max}(n)$, which corresponds to the simultaneous detection of n photons. Dependence of $SDE_{n\_pulse}$ $(n)$

for the detector #T1 is presented in Figure 5 by circles. Also in Figure 5 is presented the dependence $SDE_{n\_cw}$. Since the probability of each section switching at absorption of the photon is an independent event, we have found $SDE_{n\_cw}$ as

$$SDE_{n\_cw} = SDE_{1\_cw}^{n}, \quad (3)$$

by using of the measurement results $SDE_{1\_cw}$ = 86% with CW laser source. Furthermore, Figure 5 contains the $SDE_{n\_pulse}$ and $SDE_{n\_cw}$ dependencies [12] for the detector #T2 with topology #2. So, the figure 5 presents the comparison of the $SDE_{n\_cw}$ which expected from (3) with system detection efficiency $SDE_{n\_pulse}$ found from measurements with pulse source.

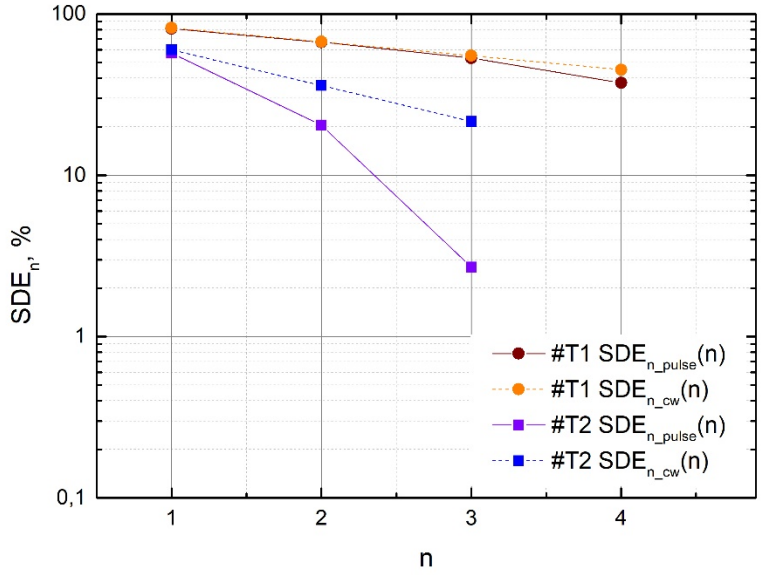


Figure 5. Dependencies $SDE_{n\_cw}(n)$ and $SDE_{n\_pulse}(n)$.

Several conclusions may be drawn from the presented graphs and from comparison of the dependencies $SDE_{n\_pulse}$ and $SDE_{n\_cw}$. The indicated dependencies for sample #T1 almost completely coincide, excluding minor differences that are visible only for n = 4, and sample #T2 shows significant differences, starting at n = 2. We believe that this is due to the fact that all four sections of detector #T1 worked identically (had the same η values), unlike detector #T2, where the spread of the η's may be significant. This spread, in our opinion, may be explained partly by the mismatch between the radiation and each section of the detector caused by the spatial inhomogeneity of the radiation at the output of the single-mode fiber, which obeys the Gaussian distribution. This mismatch should correspond to detector topology #2 (sample #T2) and be absent in detector topology #1 (#T1), which is indeed the case in the experiment. However, such a significant difference between $SDE_{n\_pulse}$ and $SDE_{n\_cw}$ cannot be explained by the topology of the sensitive element of detector #T2 alone. Apparently, there is also some non-homogeneity of detection efficiency across sections, which could be connected, for example, with some constriction in one of the detector sections.

Also, we tried to examine the dependence of the number of counts vs. the trigger level (presented in Figure 4) with the values $M_{th}(n) = \sum_{i=n}^{k,k\geq n} N_{th}(i)$ obtained on the basis of the relation (1) and taking into account the measurement of $SDE_{1\_cw}$ for detector #T1. The calculated values $M_{th}(n)$ are presented in Figure 4 as black bars with $SDE_{1\_cw}$ = 86% and $\eta = SDE_{1\_cw}/4$. The obtained experimental results show good agreement with our calculation so

for μ= 2 we had error 4%, 5.7%, 7%, 37% for photon numbers 1, 2, 3, 4. For 4 photons we observed higher error. Possible reason of it is imperfection work of our model in case when n=k and possible not so identical of DE for different sections.

### *4.2 Jitter*

The 4-PNR detector jitter was measured using the method described in [15] with a TCSPC SPC-150NX (B&H) and pulsed laser (pulse duration 1 ps, wavelength 1550 nm). The laser power corresponded to an average photon number of 0.1 per pulse, so the prevailing number of voltage pulses from the SSPD detector corresponded to the detection of single photons and the multiphoton operation of the detector was negligible. The measurement results are presented in Figure 6. The measured FWHM jitter value was 90.7 ps.

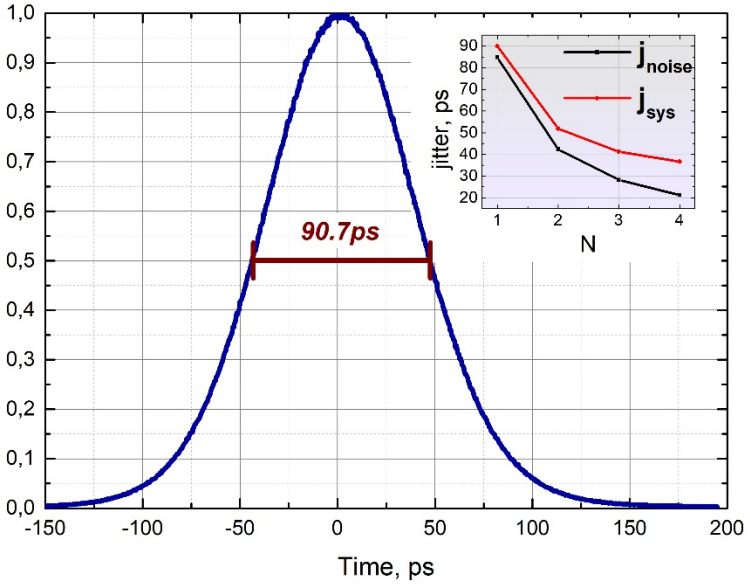


Figure 6. Jitter 4-PNR SSPD.

Currently, the best jitter values of single-pixel SSPDs published in the literature are < 20 ps [15, 16]. The jitter produced by a narrow and short superconducting strip when detecting photons has been also investigated in the work [17] and reaches 3 ps, which, at the moment, is the lowest value published for any SSPD.

In a number of works [15, 16, 18, 19, 20] whose authors study the factors influencing the value of the measured jitter, it is shown that the jitter ($j_{sys}$) measured in the experiment can be represented as the sum of several components:

$$j_{sys} = \sqrt{j^2_{noise} + j^2_{setup} + j^2_{\text{int}}}, \quad (4)$$

where $j_{setup}$ is the jitter introduced by the measuring electronics and the laser, $j_{int}$ is the SSPD's own jitter, $j_{noise}$ is the jitter that occurs when the pulse from the SSPD passes through the amplification circuit, and $j_{noise}$ may be expressed as:

$$j_{noise} = 2\sqrt{2\ln(2)} \cdot \frac{\sigma RMS}{SR}, \quad (5)$$

where σRMS is the rms noise of the amplifiers, and SR is the slew rate of the pulse edge. The slew rate parameter SR is defined as SR = max (ΔV/Δt), where ΔV and Δt are the amplitude of the voltage pulse and the rise time of this pulse, respectively. Substitution of the values obtained in our measurements into the expression (σRMS = 5.6 mV, ΔV = 70 mV, and Δt = 450 ps) allows us to calculate the jitter connected with the amplification circuit as $j_{noise}$ =

84.6 ps. Thus, $j_{noise}$ is the key parameter in our experiments and is apparently associated with a rather small amplitude of the voltage pulse. So, the calculated value of the SSPD intrinsic jitter is $j_{int}$ = 30.7 ps, which is typical for traditional SSPD receivers. Using expressions (4), (5), and the obtained value of $j_{int}$, we calculated values for $j_{noise}$ and $j_{sys}$ in which the pulse amplitude corresponds to 2-, 3- and 4-photon operations (inset in Figure 6). The expected system jitter values for these multiphoton operations were 52 ps, 41 ps, and 36 ps, respectively. Further improvement of the system jitter is possible via using cooled amplifiers, which have lower noise, and detectors with a higher critical current value.

## 5. Summary

The 4-PNR SSPD with high SDE, approaching the record values of traditional single-section superconducting single-photon detectors, was presented for the first time. A complete characterization of 4-PNR SSPD detectors was carried out. Further, the possibility of reconstructing the radiation source statistics using the created 4-PNR SSPD was demonstrated. A comparison of the created 4-PNR SSPD with other types of PNR detectors and non-PNR detectors operating in PNR mode currently available is presented in Table 1. The main advantage of our 4-PNR detector is that it works without of any multiplexing scheme with one coaxial line, a SDE, a high timing resolution (low jitter), a low dark counts rate, and an ultralow dead time.

**Table 1. PNR Single-photon detectors at λ=1550 nm**

| Detector type | SDE, % | Temperature, K | Jitter, ps | Dead Time, ns | Dark Counts, cps | Reference |
|---|---|---|---|---|---|---|
| 4-PNR SSPD | 86 | 2 | 90 | 2 | 35 | This article |
| TES | 95 | 0.1 | 25000 | 200 | 500 | [21-23] |
| PMT | 2 | 200 | 367 | 100 | 5000 | [24] |
| SPAD | 25 | 173 | 55 | 200 | 100 | [25-28] |

## 6. Funding

This work was supported by the Russian Science Foundation under grant № 18-12-00364.

## References

1. G. Gol'tsman, O. Okunev, G. Chulkova, A. Lipatov, A. Semenov, K. Smirnov, C. Williams and R. Sobolewski, "Picosecond superconducting single-photon optical detector," Appl. Phys. Lett.**79**(6), 705-707 (2001).
2. T. Yamashita, S. Miki and H. Terai, "Simulation of heat propagation processes in the detection pixel with superconducting layers of single-photon thermoelectric detector," IEICE Transactions on Electronics **100**(3), 274-282 (2017).
3. F. Marsili, V. B. Verma, J. A. Stern, S. Harrington, A. E. Lita, T. Gerrits, I. Vayshenker, B. Baek, M. D. Shaw and R. P. Mirin, "Thin-Film thermal conductivity measurements using superconducting nanowires," Nature Photonics **7,** 210-214 (2013).
4. K. Smirnov, A. Divochiy, Y. Vakhtomin, P. Morozov, P. Zolotov, A. Antipov and V. Seleznev, "NbN single-photon detectors with saturated dependence of quantum efficiency," Superconductor Science and Technology **31**(3) 035011 (2018).
5. D. Rosenberg, A. Kerman, R. Molnar and E. Dauler, "High-speed and high-efficiency superconducting nanowire single photon detector array," Opt. Express **21**, 1440 (2013)
6. A. Divochiy, F. Marsili, D. Bitauld et.al. "Superconducting nanowire photon-number-resolving detector at telecommunication wavelengths," Nature Photonics **2**, 302-306(2008).
7. F. Marsili, D. Bitauld, A. Gaggero, S. Jahanmirinejad, R. Leoni, F. Mattioli and A. Fiore, "Physics and application of photon number resolving detectors based on superconducting parallel nanowires" New Journal of Physics," **11**, 045022 (2009).
8. F. Mattioli, Z. Zhou, A. Gaggero, R. Gaudio, S. Jahanmirinejad, D. Sahin, F. Marsili, R. Leoni and A. Fiore "Photon-number-resolving superconducting nanowire detectors," Superconductor Science and Technology **28**(10), 104001 (2015).
9. U. M. Maurer, "Secret key agreement by public discussion from common information," IEEE Trans. Inf. Theory **39**, 733–742 (1993).

10. Marco Cattaneo, Matteo G. A. Paris and Stefano Olivares, “Hybrid quantum key distribution using coherent states and photon-number-resolving detectors,” Phys. Rev. A, 98(1), 012333 (2018).
11. M. Ejrnaes, R. Cristiano, O. Quaranta, S. Pagano, A. Gaggero, F. Mattioli, R. Leoni, B. Voronov, and G. Gol’tsman, “A cascade switching superconducting singlephoton detector,” Appl. Phys. Lett. **91**, 262509 (2007).
12. P. Zolotov, A. Divochiy, Yu. Vakhtomin, M. Moshkova, P. Morozov, V. Seleznev, and K. Smirnov, “Photon-number-resolving SSPDs with system detection efficiency over 50% at telecom range,” AIP Conference Proceedings **1936**, 020019 (2018).
13. K. Smirnov, Y. Vachtomin, A. Divochiy, A. Antipov and G. Goltsman, “Dependence of dark count rates in superconducting single photon detectors on the filtering effect of standard single mode optical fibers,” Applied Physics Express **8**(2), 022501 (2015).
14. H. Paul, P. Törmä, T. Kiss, I. Jex, “Photon chopping: New way to measure the quantum state of light,” Physical review letters **76**(14), 2464 (1996).
15. V. Shcheslavskiy, P. Morozov, A. Divochiy, Yu. Vakhtomin, K. Smirnov and W. Becker, “Ultrafast time measurements by time-correlated single photon counting coupled with superconducting single-photon detector,” Rev. Sci. Instrum **87**(5), 053117 (2016).
16. Iman Esmaeil Zadeh, Johannes W. N. Los, Ronan B. M. Gourgues, Violette Steinmetz, Gabriele Bulgarini, Sergiy M. Dobrovolskiy, Val Zwiller, and Sander N. Dorenbos, “Single-photon detectors combining high efficiency, high detection rates, and ultra-high timing resolution,” APL Photonics, **2**(11), 111301(2017).
17. B.A. Korzh, Q.Y. Zhao, S. Frasca, J.P. Allmaras, T.M. Autry, E.A. Bersin, M. Colangelo, G.M. Crouch, A.E. Dane, T. Gerrits et al., “Demonstrating sub-3 ps temporal resolution in a superconducting nanowire single-photon detector,” arXiv preprint arXiv:1804.06839, (2018).
18. F. Najafi, A. Dane, F. Bellei, Z. Qingyuan, K. A. Sunter, A. N. McCaughan, and K. K. Berggren, “Fabrication process yielding saturated nanowire single-photon detectors with 24-ps jitter,” IEEE Journal on Selected Topics in Quantum Electronics, **21**(2), 1–8 (2015).
19. Lixing You, Xiaoyan Yang, Yuhao He, WenxingWeijun Zhang, Dengkuan Liu, WenxingWeijun Zhang, Lu Ling Zhang, Lu Ling Zhang, 2 Xiaoyu Liu, Sijing Chen, Zhen Wang and XiaomingXie, “Jitter analysis of a superconducting nanowire single photon detector,” AIP Advances **3**(7), 4–10 (2013).
20. M. Caloz, M. Perrenoud, C. Autebert, B. Korzh, M. Weiss C. Schönenberger, Richard J. Warburton, H. Zbinden, and F. Bussières, “High-detection efficiency and lowtiming jitter with amorphous superconducting nanowire single-photon detectors,” Appl. Phys. Lett. **112**(6), 061103 (2018).
21. A.J. Miller, S.W. Nam, J.M. Martinis and A. Sergienko, “Demonstration of a low-noise near-infrared photon counter with multiphoton discrimination,” Appl. Phys. Lett. **83**(4), 791-793 (2003).
22. A. E. Lita, A. J. Miller, and S. W. Nam, “Counting near-infrared single-photons with 95% efficiency,” Opt. Express **16**(5), 3032-3040 (2008).
23. R. Hadfield and G. Johansson, “Superconducting Devices in Quantum Optics,” Springer, 43 (2016).
24. Thermoelectric cooled NIR-PMT Hamamatsu #H12397-75
25. IDQuantique ID230 https://www.idquantique.com/single-photon-ystems/products/id230/
26. B. E. Kardynał, Z. L. Yuan and A. J. Shields, “An avalanche□photodiode-based photon-number-resolving detector,” Nature Photonics **2**, 425–428 (2008).
27. M. J. Fitch et al., “Photon-number resolution using time-multiplexed single-photon detectors,” Phys. Rev. A **68**, 043814 (2003).
28. A.R. Dixon, Z.L. Yuan, J.F. Dynes, A.W. Sharpe and A.J. Shields, “Gigahertz decoy quantum key distribution with 1 Mbit/s secure key rate,” Opt. Express **16**, 18790–18797 (2008).